Journal of Photochemistry and Photobiology A: Chemistry 200 (2008) 141–147

Contents lists available at ScienceDirect

Journal of Photochemistry and Photobiology A: Chemistry

journal homepage: www.elsevier.com/locate/jphotochem

Visible-light-driven boron/ferrum/cerium/titania photocatalyst

Qincai Ling, Jianzhong Sun*, Qiyun Zhou, Qian Zhao, Hua Ren

State Key Laboratory of Chemical Engineering, Department of Chemical and Biochemical Engineering, Zhejiang University, Zheda Road, Hangzhou 310027, China

ARTICLE INFO

Article history:
Received 16 July 2007
Received in revised form 20 March 2008
Accepted 2 July 2008
Available online 11 July 2008

Keywords:
Titania
Boron
Ferrum
Cerium
Visible light photocatalysis

ABSTRACT

A boron/ferrum/cerium/titania photocatalyst with visible-light-induced performance was prepared by the conventional sol–gel method, in which tetrabutyl titanate ($Ti(O\text{-}nC_4H_9)_4$) was used as the precursor and boric acid (H_3BO_3), ferric nitrate enneahydrate ($Fe(NO_3)_3{\cdot}9H_2O$), and cerium nitrate hexahydrate ($Ce(NO_3)_3{\cdot}6H_2O$) were the sources of boron, ferrum, and cerium, respectively. The microstructure and optical property of the photocatalyst were characterized by X-ray diffraction (XRD), X-ray photoelectron spectroscopy (XPS), scanning electron microscopy (SEM), N_2 adsorption–desorption isotherm, and UV–vis diffusive reflectance spectroscopy (DRS). It was found that the as-prepared photocatalyst composed of anatase and that the presence of impurities could retard phase transformation of TiO_2 from anatase to rutile at elevated temperatures and could prohibit growth of polycrystalline, which favored forming photocatalyst with large surface area. Degradation of 2,4-dichlorophenol (DCP) under visible light illumination was used to evaluate the photocatalytic activity. Comparative investigations showed that photocatalytic performance of the boron/ferrum/cerium/titania photocatalyst was the highest among the all test samples. It was testified that boron doping led to the band gap narrow and the response to visible light, and that ferrum and cerium impurities, which presented in the forms of FeO/Fe_2O_3 and Ce_2O_3/CeO_2, dispersed on the surface of TiO_2, suppressed the electron and hole recombination, and resulted in the enhancement of catalytic performance. The results exhibited that the synergistic effects of boron, ferrum and cerium played an important role in the band gap narrow and the increase of photoactivity.

1. Introduction

In the past decades, photocatalysis has become an area of great research interest because of serious pollution in the environment from industrial and agricultural wastes, which contain harmful organic compounds. Among various kinds of photocatalysts, TiO_2 is widely used to photo-degrade a great deal of pollutants because of its excellent properties, such as cheapness, nontoxicity, structural stability, abundance, high oxidation rate and ecological friendliness [1–11]. However, there are some significant limitations for titania photo-degradation and the major constraint is its low photoquantum efficiency resulting from low interfacial charge-transfer rate of photo-generated carriers and high recombination of photo-induced electron–hole pairs [2,12]. Moreover, titania with the high energy band gap (ca. 3.0 eV for rutile and 3.2 eV for anatase) can be activated only by ultraviolet (UV) light, thus basically ruling out the use of sunlight which contains less than 5% UV light as the light source for the photocatalysis and making it seemingly improbable to take advantage of the solar energy [6,9]. Therefore, the modification to titania has attracted great attention to improve the response of titania to visible light and enhance the separation of electron–hole pairs for the purpose of preparing the novel photocatalysts which show the high activity under visible light irradiation as well as utilizing effectively sunlight. Numerous methods, such as loading noble metal over semiconductor photocatalyst [13], using rare earth metal [12] or transition metal [14] as impurities, photosensitizing titania [15], compounding titania with other materials[16], doping of titania with nonmetal [6–10] have been investigated. Of these approaches for modification to TiO_2, using metal or nonmetal as impurity has been frequently performed and many reports have also been published on the field. Previous studies demonstrated that the metal ions could trap temporarily the photo-generated charge carriers and could inhibit the recombination of photo-induced electron–hole pairs when migrating from the inside of the photocatalyst to the surface [12], whereas the doping with nonmetal could narrow the band gap and might drive the photocatalytic performance under the visible light [6–10]. It was proved that modification to titania by the synergistic effects was an effective method for increasing the photocatalytic activity, too. Zhao et al. [17] reported that $Ni_2O_3/TiO_{2-x}B_x$ photocatalyst was prepared by a simple method of modified sol–gel and that the improvement in both spectral response and photocatalytic efficiency could

* Corresponding author. Tel.: +86 571 87953171; fax: +86 571 87951612.
E-mail address: bigwig@zju.edu.cn (J. Sun).

1010-6030/$ – see front matter © 2008 Elsevier B.V. All rights reserved.
doi:10.1016/j.jphotochem.2008.07.003

be achieved through a combined approach doping with nonmetal boron and loading the metal oxide Ni_2O_3. They demonstrated that incorporation of B into TiO_2 could extend the spectral response to the visible region and that the photocatalytic activity was greatly enhanced when it was further loaded with Ni_2O_3. Sakatani et al. [18] reported that La–N–TiO_2 photocatalyst, which could decompose acetaldehyde under visible light irradiation, was prepared by means of polymerized method. Yuan et al. [19] revealed the cooperative action of Zn^{2+} and Fe^{3+} over titania could obviously improve the photocatalytic performance for the phenol degradation. Li et al. [20] prepared the N–F co-doped photocatalyst by pyrolysis method and pointed out that its high Vis photocatalytic activity was ascribed to a synergetic effect of its unique surface characteristics, doped N atoms, and doped F atoms. These investigations indicate that the synergistic effects can obviously increase the photocatalytic activity of TiO_2. It is worth noticing that the mechanisms of modification using metal and nonmetal element are completely different, and that metal atoms either form individual phases dispersed into TiO_2 or accommodate into the lattices of TiO_2, which are primarily related to metal ion radii [12,21] while nonmetal atoms can enter into TiO_2 lattice [6–10,17]. It is expected that the synergistic effects of transition metal, rare earth metal and nonmetal can be used to raise the photoactivity. However, to the best of our knowledge, report on this aspect has not been found so far among the impressive number of publications. On the basis of the consideration, we carried out the investigation on photocatalysis and succeeded in preparing boron/ferrum/cerium/titania photocatalyst by the sol–gel route. The as-prepared titania samples were characterized by XRD, XPS, DRS, SEM, N_2 adsorption–desorption isotherm. The decomposition of DCP under visible illumination was used as a probe reaction to evaluate the photocatalytic property. The effects of impurities on photocatalytic activity were investigated in detail and the reasons for exhibiting Vis photocatalytic activity in this system were elucidated.

2. Experimental

2.1. Photocatalyst preparation

All chemicals used in this study, in which tetrabutyl titanate was chemically pure and others were analytically pure, were used as received without any further purification. Water used was deionized water. In order to prepare the photocatalyst by means of the sol–gel technique, two kinds of solutions (solutions 1 and 2) were prepared first. Solution 1 was made by the following procedures, which 0.002 mol boric acid (H_3BO_3), 0.002 mol ferric nitrate enneahydrate ($Fe(NO_3)_3{\cdot}9H_2O$), and 0.002 mol cerium nitrate hexahydrate ($Ce(NO_3)_3{\cdot}6H_2O$) were dissolved in 20 mL of water (H_2O) at room temperature, and 15 mL of glacial acetic acid (CH_3COOH) and 80 mL of ethanol (CH_3CH_2OH) were added. Solution 2 was obtained by the following method, which 0.1 mol tetrabutyl titanate ($Ti(O\text{-}nC_4H_9)_4$) was dissolved in 80 mL of anhydrous ethanol. Then, the solution 2 was added drop-wise into the solution 1 within 60 min using a separating funnel, keeping the reaction mixture vigorously magnetically stirred to form the sol. Subsequently, the sol was stirred continuously for 2 h and aged for 72 h at room temperature to prepare the gel. The resulting gel was dried for 12 h at 100 °C under reduced pressure to gain the xerogel, which was crushed to obtain powder, followed by annealing at desired temperature for 2 h to remove the residual organic compounds resulting from the hydrolysis of the $Ti(O\text{-}nC_4H_9)_4$ and the solvent to prepare boron/ferrum/cerium/titania photocatalyst. The as-prepared sample was kept in a vacuum until the time of use. The sample was labeled as B–Fe–Ce–TiO_2-*X*, where B–Fe–Ce represented impurities of boron, ferrum, and cerium, and X denoted the corresponding temperature of calcination. Other samples, including B–Fe–TiO_2-500, B–Ce–TiO_2-500, Fe–Ce–TiO_2-500, Ce–TiO_2-500, B–TiO_2-500, Fe–TiO_2-500, and undoped TiO_2-500 as well as B–Fe–Ce–TiO_2-400, B–Fe–Ce–TiO_2-450, B–Fe–Ce–TiO_2-550, B–Fe–Ce–TiO_2-600 and undoped TiO_2-600, were synthesized in the same procedures changing the component of solution 1 or calcination temperature for the purpose of the comparative tests. The procedures of preparing the photocatalyst were represented in Fig. 1.

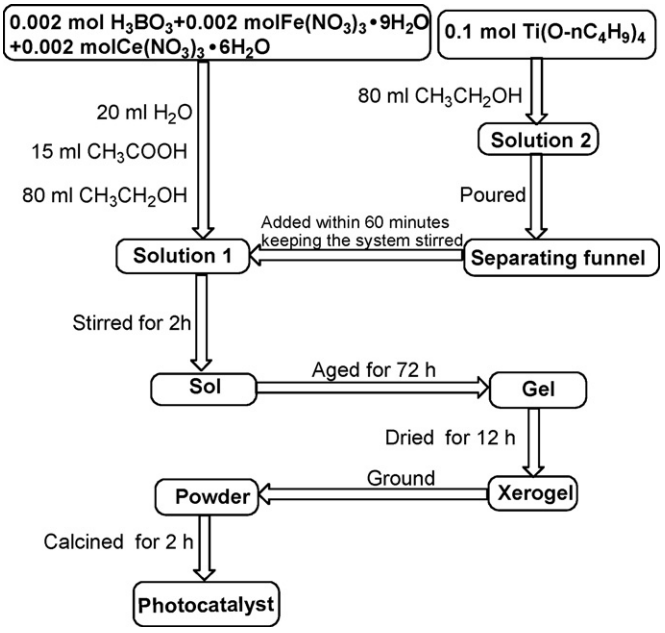

Fig. 1. Procedures of preparing the boron/ferrum/cerium/titania photocatalyst.

2.2. Photocatalyst characterization

The XRD patterns recorded on a D/max-RA X-ray diffractometer with Cu target Kα radiation (λ = 0.15406 nm) as X-ray source at a scan speed of 2° min^{-1} in a 2θ range of 20–80° were used to contrast the standard diffraction charts of anatase and rutile, determine the crystallite size, and calculate the lattice parameters. The accelerating voltage and the applied current were 40 kV and 100 mA, respectively. Crystallite sizes were determined through the widths of half-height according to the Scherrer equation.

The oxidation states of atoms at the surface of TiO_2 were analyzed using the binding energies from X-ray photoelectron spectroscope (XPS). The XPS spectra of the synthesized photocatalyst were recorded by a Thermo Escalab250 X-ray photoelectron spectroscope equipped with Al Kα excitation. Detailed scans were recorded for B 1s, Fe 2p, Ce 3d, and Ti 2p. The C 1s peak set at 284.6 eV was used as an internal reference for absolute binding energies.

The UV–vis diffusive reflectance spectra of the as-prepared samples in the wavelength range of 200–800 nm were determined using a Shimadzu (Japan) DUV-3700 UV–vis–NIR Recording Spectrophotometer with an integrating sphere. $BaSO_4$ was used to be a reference.

The surface morphologies and the particle size of photocatalysts were observed and estimated by means of a S-4800 Scanning Electron Microscope (Hitachi).

The N_2 adsorption–desorption isotherms were determined by Autosorb-1 at 77 K. Prior to measurements, the samples were outgassed in an evacuation chamber for 8 h at 423 K.

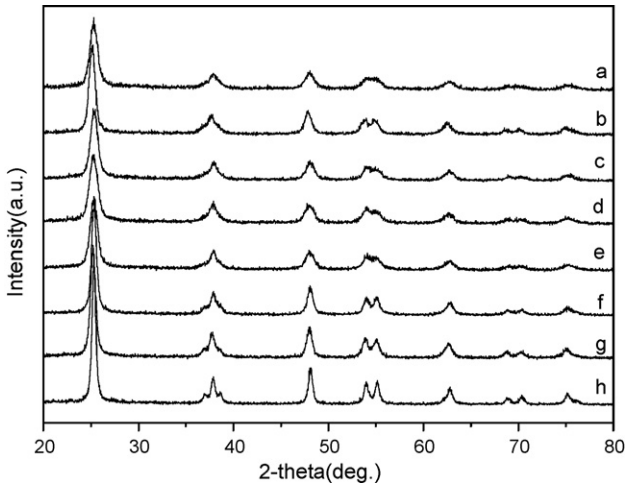

Fig. 2. XRD patterns: (a) B–Fe–Ce–TiO_2-500, (b) B–Fe–TiO_2-500, (c) B–Ce–TiO_2-500, (d) Fe–Ce–TiO_2-500, (e) Ce–TiO_2-500, (f) B–TiO_2-500, (g) Fe–TiO_2-500, and (h) undoped TiO_2-500.

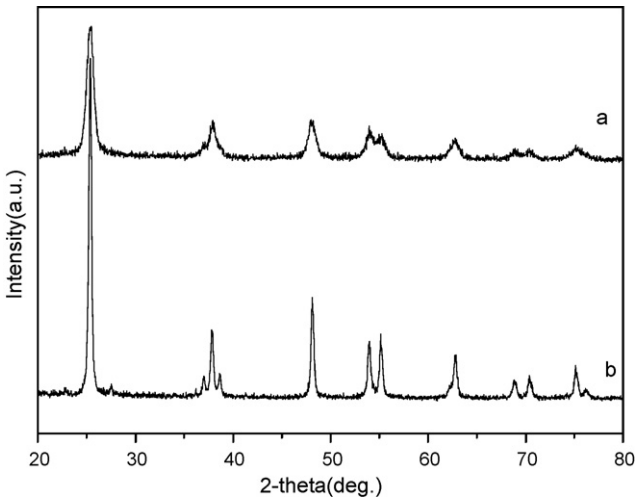

Fig. 3. XRD patterns: (a) B–Fe–Ce–TiO_2-600 and (b) undoped TiO_2-600.

2.3. Photocatalytic activity test

2,4-Dichlorophenol (DCP), which was a common chemical used extensively in a variety of industrial and agricultural applications, was chosen as model pollutant to evaluate the photocatalytic performance. The degradation of DCP was conducted in a 100 mL of self-designed quartz vessel with a suspension containing 50 mL of 10 mg/L DCP (the initial concentration C_{in}) solution and 0.05 g of photocatalyst. In order to keep the temperature of photoreaction constant, the reactor was immersed in a thermostatic circulation bath (30.0 °C). In the process of decomposition, the reaction system was exposed in the air, keeping the reaction mixture magnetically stirred. A 50-W metal halide lamp located at 5 cm above the reactor provided the light source, which was filtered by a 410-nm cut filter (L41, KenKo Japan) to assure cut-off of the UV light. Prior to illumination, the suspension was ultrasonicated for 5 min and stirred for 30 min in the dark to allow the adsorption of DCP reach a state of equilibrium. Then, 5 mL of suspension was withdrawn by sucker and centrifuged at 12,000 rpm for 10 min. The centrifugate was used to determine the initial absorbance (A_0). After determination, the clear solution tested and the cloudy suspension remained were rapidly poured into the vessel. The decomposition experiment was carried out for 3 h and the reaction mixture was periodically sampled every hour to analyze the absorbance (A), which was determined at the characteristic wavelength, indicated the maximal absorption peak of DCP at $\lambda = 285.5$ nm by a 751GD UV–vis spectrophotometer. The photocatalytic activity is evaluated by

$$\text{Degradation ratio} = \frac{C_0 - C}{C_0} \times 100\% = \frac{A_0 - A}{A_0} \times 100\% \quad (1)$$

where C_0 and C represent the concentration at the adsorption equilibrium and the concentration at irradiation time t, respectively; A_0 and A represent the absorbance at the adsorption equilibrium and the absorbance at irradiation time t, respectively.

3. Results and discussion

3.1. XRD spectra of samples

The XRD patterns of different samples, including B–Fe–Ce–TiO_2-500, B–Fe–TiO_2-500, B–Ce–TiO_2-500, Fe–Ce–TiO_2-500, Ce–TiO_2-500, B–TiO_2-500, Fe–TiO_2-500, and undoped TiO_2-500 are shown in Fig. 2. Compared with the 21-1272 anatase ASTM (American Society for Testing and Materials) card and the 21-1276 rutile ASTM card, it could be observed that the all samples were present in the anatase phases when annealed at 500 °C for 2 h and that there was no evident difference between them and anatase TiO_2. Furthermore, it could be estimated that the average particle sizes were 9.6, 11.8, 9.9, 9.8, 11.5, 14.0, 13.5, and 17.6 nm for B–Fe–Ce–TiO_2-500, B–Fe–TiO_2-500, B–Ce–TiO_2-500, Fe–Ce–TiO_2-500, Ce–TiO_2-500, B–TiO_2-500, Fe–TiO_2-500, and undoped TiO_2-500, respectively. Obviously, the smallest average particle was for B–Fe–Ce–TiO_2-500 and the biggest average particle was for undoped TiO_2-500 among these samples. The XRD patterns of B–Fe–Ce–TiO_2-600 and undoped TiO_2-600 are shown in Fig. 3. It could be observed that B–Fe–Ce–TiO_2-600 consisted only of anatase phase while undoped TiO_2-600, which a weak peak occurred at $2\theta = 27.4°$ (1 1 0) for rutile, existed in the states of both anatase and rutile. The results revealed that the impurities could prohibit growth of polycrystalline and could retard the transformation from anatase to rutile at elevated temperatures.

In addition, the analysis from XRD revealed that the Fe and Ce did not incorporate into the lattice of TiO_2, and that B was weaved into the crystal lattice of TiO_2. In fact, it was demonstrated that ferric nitrate enneahydrate and cerium nitrate hexahydrate were changed into FeO/Fe_2O_3 and Ce_2O_3/CeO_2 in the process of the calcination by XPS (3.2). The ionic radii of Ce^{3+}, $Ce^{4+}$and Ti^{4+} are 0.101, 0.087, and 0.068 nm, respectively. Therefore, it can be deduced theoretically that Ce^{3+} and Ce^{4+} cannot be weaved into the lattice of TiO_2. However, there were no separate phases of FeO/Fe_2O_3 and Ce_2O_3/CeO_2 to be detected and the possible reason was that their amounts were less than limits of detection of the instrument.

3.2. XPS spectra of boron/ferrum/cerium/titania photocatalyst

The XPS spectra of B–Fe–Ce–TiO_2-500 for B 1s, Fe 2p, Ce 3d, and Ti 2p are shown in Figs. 4–7, respectively. From Fig. 4, it could be seen that the binding energy (BE) for B 1s was 191.8 eV. Based on the previous researches reported in the literature, the binding energies (BEs) for B 1s were 193.6 eV in B_2O_3 [22], 193.0 eV in H_3BO_3 [23], and 187.5 eV in TiB_2 [24], respectively. This indicated that the boron atoms were bonded by means of neither B–Ti–B bond nor B–O bond. BEs for B 1s in FeB and Fe_2B were 187.9 eV [24] and 188.3 eV[25], respectively. Fig. 5 revealed that BE for Fe 2p was 710.3 eV, assigned to Fe $2p_{3/2}$. BEs for Fe $2p_{3/2}$ in FeB, Fe_2B, FeO, and Fe_2O_3 were 707.4 eV [24], 707.3 eV [25], 709.6 eV [26] and 710.9 eV [27], respectively. Undoubtedly, on one hand, there was no existence of the

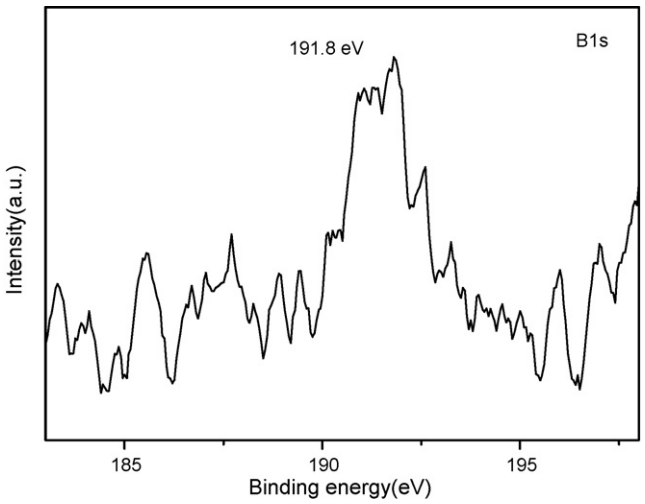

Fig. 4. XPS spectra of B–Fe–Ce–TiO_2-500 for B 1s.

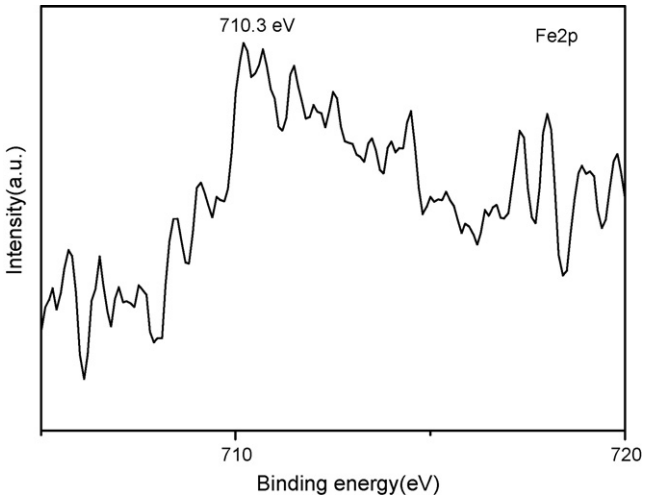

Fig. 5. XPS spectra of B–Fe–Ce–TiO_2-500 for Fe 2p.

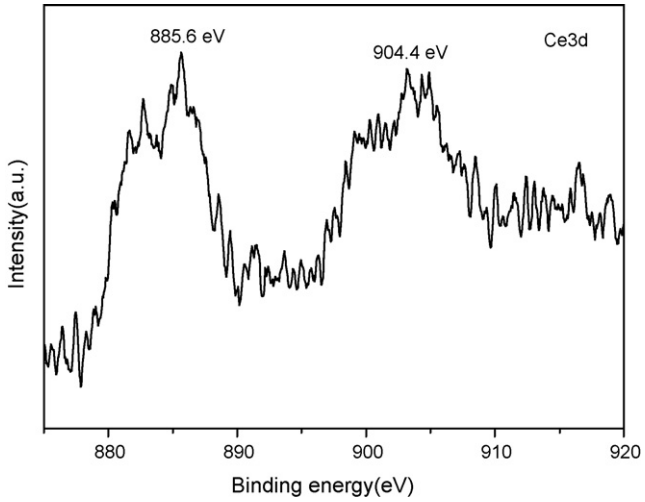

Fig. 6. XPS spectra of B–Fe–Ce–TiO_2-500 for Ce 3d.

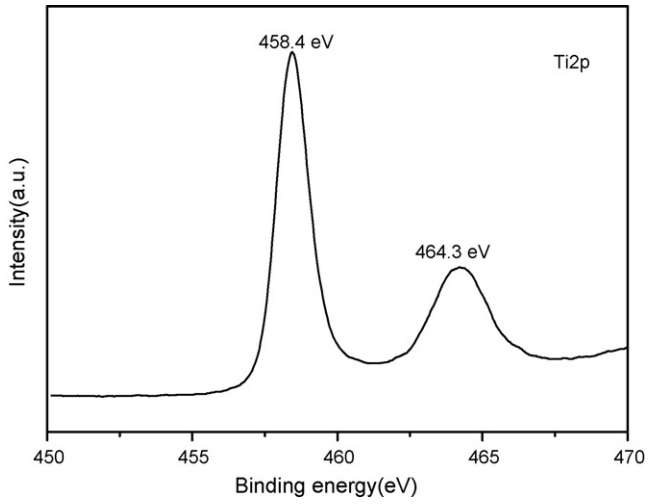

Fig. 7. XPS spectra of B–Fe–Ce–TiO_2-500 for Ti 2p.

compounds FeB or Fe_2B, either. On the other hand, the broad XPS spectra for Fe $2p_{3/2}$ (BE = 710.3 eV) suggested the presence of FeO and Fe_2O_3 [26,27]. Fig. 6 revealed the quite broad XPS spectra of Ce 3d and that BEs for Ce 3d were 885.6 eV and BE = 904.4 eV, which should be attributed to Ce $3d_{5/2}$ and Ce $3d_{3/2}$ in Ce_2O_3 or CeO_2 according to the literature [28,29]. Therefore, it was not difficult to imagine that Ce existed in the forms of Ce_2O_3 or CeO_2. According to the report [24], BE for Ti $2p_{3/2}$ in TiB_2 was 454.4 eV, thus confirming further that there were no existences of the compound TiB_2. BE = 458.4 eV and BE = 464.3 eV for Ti 2p should be attributed to Ti $2p_{3/2}$ and Ti $2p_{1/2}$ of TiO_2, indicating that Ti remained in an octahedral environment. Undoubtedly, the boron atom was doped into TiO_2 lattice, possibly holding such a chemical structure as B–Ti–O. The ferrum and cerium atoms existed in the forms FeO/Fe_2O_3 and Ce_2O_3/CeO_2. The XPS analysis also showed that molar ratio of Ti:B:Fe:Ce for as-prepared B–Fe–Ce–TiO_2-500 were 1:0.021:0.037:0.035. However, B–Fe–Ce–TiO_2-500 was prepared in terms of the corresponding ratio of Ti:B:Fe:Ce = 1:0.02:0.02:0.02. This revealed that FeO/Fe_2O_3 and Ce_2O_3/CeO_2 were dispersed on the surface of TiO_2. In order to further verify the oxidation states of the atoms, samples of B_2O_3, H_3BO_3, TiB_2, Fe_2O_3, Ce_2O_3 were used as standards to determine the binding energies. It was found that BEs were 193.5 eV for B 1s in B_2O_3, 193.4 eV for B 1s in H_3BO_3, 187.9 eV for B 1s in TiB_2, 710.5 eV for Fe $2p_{3/2}$ in Fe_2O_3, and 886.0 eV for Ce $3d_{5/2}$ in Ce_2O_3. The results were in agreement with the reports in the literature [22–24,27,28] and supported the analysis of the XPS spectra. In addition, these results further testified the conclusions from the analysis of the XRD spectra of B–Fe–Ce–TiO_2-500, too.

3.3. UV–vis DRS spectra of typical samples

The as-prepared boron/ferrum/cerium/titania photocatalyst was vivid yellow. Generally, the color of a solid is determined by the position of its absorption edge and a shift of this absorption edge toward higher wavelength can result in absorption in the visible part of the spectrum. The optical absorption spectra of B–Fe–Ce–TiO_2-500, B–TiO_2-500, Ce–TiO_2-500, Fe–TiO_2-500, and undoped TiO_2-500 powder are shown in Fig. 8. In comparison with undoped TiO_2-500, there was strong photoabsorption in the visible region for B–Fe–Ce–TiO_2-500 and B–TiO_2-500. However, there was hardly Vis absorbance for Ce–TiO_2-500 or Fe–TiO_2-500. The red shift of the absorption edge implied that the band gap energy decreased, the sample could absorb more photons, and eventually photoactivity increased. From Fig. 8, it could be seen

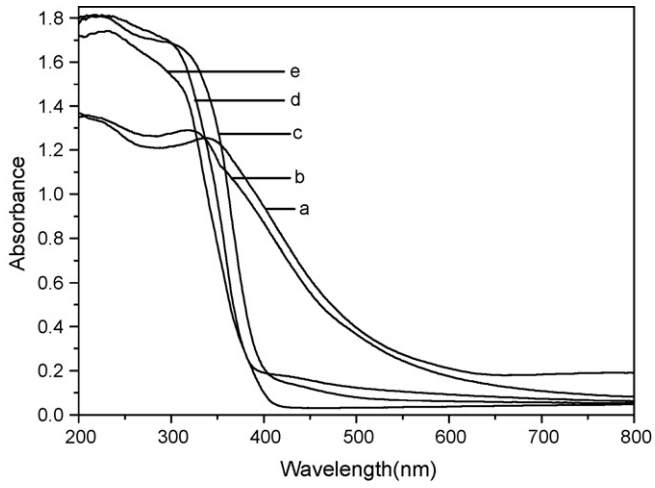

Fig. 8. Diffuse reflectance absorption spectra: (a) B–Fe–Ce–TiO_2-500, (b) B–TiO_2-500, (c) Ce–TiO_2-500, (d) Fe–TiO_2-500, and (e) undoped TiO_2-500.

that B doping could lead to the band gap narrow while Fe or Ce impurity decreases hardly the band gap. According to the results from XRD and XPS analysis, it was clear that B doping led to a modification of the electronic structure around the conduction band edge of TiO_2, and eventually resulted in the visible light response. In fact, in TiO_2 crystal the valence band (VB) and conduction band (CB) consist of both the Ti 3d and O 2p orbitals. The Ti 3d orbital is split into two parts, and the CB is divided into the lower and upper parts. When TiO_2 is doped with B, the B 2p states are somewhat delocalized, thus resulting in the modification of the electronic structure around the conduction band edge of TiO_2. The mixing of the B 2p states with VB increases the width of the VB itself. This gives rise to a decrease in the band gap energy [30]. Zhao et al. [17] calculated theoretically densities of states (DOSs) for the O substitution case, and revealed that the mixture of p orbital of B with O 2p orbital is responsible for the band gap narrow. Yang et al. [31] investigated the electronic and optical properties of several possible B-doped models, and pointed out that the transition of excited electrons from the valence band to the empty gap states above the Fermi level might be responsible for the redshift of the absorption edge in substitutional B- to O-doped anatase.

3.4. SEM photographs of B–Fe–Ce–TiO_2-500 and undoped TiO_2-500

The SEM photographs of boron/ferrum/cerium/titania and undoped TiO_2 are shown in Figs. 9 and 10, respectively. From these photographs, it could be also observed that B–Fe–Ce–TiO_2-500 and undoped TiO_2 were approximately present in the form of spherical particle. According to statistics, the average sizes of B–Fe–Ce–TiO_2 and undoped TiO_2 were about 11.2 and 17.0 nm, which were in accordance with the above-mentioned values determined by XRD.

3.5. BET surface area and pore structure

Brunauer–Emmett–Teller (BET) surface areas calculated from the linear parts of the BET plots ($p/p_0 = 0.05–0.3$) were 83.72 m^2/g for B–Fe–Ce–TiO_2-500 and 5.5 m^2/g for undoped TiO_2-500. Total pore volume and average pore size taken from the volume of N_2 adsorbed at $p/p_0 = 0.9994$ were 0.11 cm^3/g and 5.3 nm for B–Fe–Ce–TiO_2-500, and those taken from the volume of N_2 adsorbed at $p/p_0 = 0.9951$ were 0.012 cm^3/g and 9.0 nm for undoped TiO_2-500. There was no doubt that impurities led to decrease of average pore size and increase of BET surface area. As is well known,

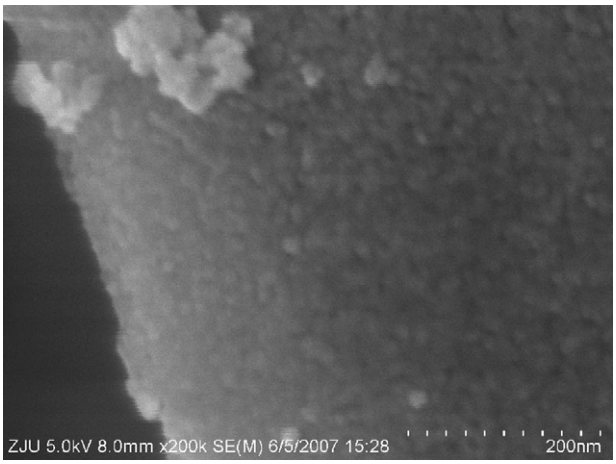

Fig. 9. SEM pattern of B–Fe–Ce–TiO_2-500.

photocatalysts with a bigger surface area are in favor of the adsorption of target pollutant.

3.6. Photocatalytic performance

DCP was used as a sacrifice reagent. The comparative tests of different samples B–Fe–Ce–TiO_2-500, B–Fe–TiO_2-500, B–Ce–TiO_2-500, Fe–Ce–TiO_2-500, Ce–TiO_2-500, B–TiO_2-500, Fe–TiO_2-500, and undoped TiO_2-500 for degradation of DCP under the identical condition were employed to evaluate the photocatalytic activity of photocatalysts. The measurements were repeated five times for each catalytic system and the results were averaged. The error in the tests was found to be within the range of 5.0%.

The adsorption of target pollutant over photocatalyst is the prerequisite of photocatalysis. Table 1 shows the concentrations of DCP at the adsorption equilibrium after 30 min in the dark over different photocatalysts. Obviously, it could be seen that the sample B–Fe–Ce–TiO_2-500 adsorbed the most amount of DCP at the adsorption equilibrium among these samples.

The decomposition ratios of DCP versus irradiation time under visible light illumination are shown in Fig. 11. It could be observed that the samples of B–Fe–Ce–TiO_2-500, B–Fe–TiO_2-500, B–Ce–TiO_2-500, and B–TiO_2-500 exhibited catalytic activity of visible light. It could be also seen that the photocatalytic activity of B–Fe–TiO_2-500 or B–Ce–TiO_2-500 was superior to the one of

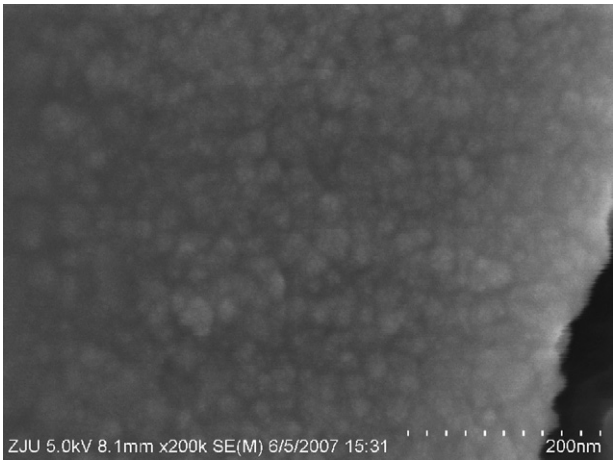

Fig. 10. SEM pattern of undoped TiO_2-500.

Table 1
The concentrations of DCP at the adsorption equilibrium after 30 min in the dark over different photocatalysts (for C_{in} = 10 mg/mL)

Sample	C_0 (mg/mL)
B–Fe–Ce–TiO_2-500	7.66
B–Fe–TiO_2-500	8.45
B–Ce–TiO_2-500	8.30
Fe–Ce–TiO_2-500	8.68
Ce–TiO_2-500	8.95
B–TiO_2-500	8.59
Fe–TiO_2-500	8.75
Undoped TiO_2-500	9.12
B–Fe–Ce–TiO_2-400	8.35
B–Fe–Ce–TiO_2-450	8.03
B–Fe–Ce–TiO_2-550	7.82
B–Fe–Ce–TiO_2-600	8.15

C_{in}, initial concentration; C_0, concentration at the adsorption equilibrium.

B–TiO_2-500, that the photocatalytic activity of B–Fe–Ce–TiO_2-500 exceeded the one of B–Fe–TiO_2-500 or B–Ce–TiO_2-500, and that the best performance was attributed to boron/ferrum/cerium/titania photocatalyst. Moreover, Fe–TiO_2-500 and Ce–TiO_2-500 hardly revealed photoatalytic performance under visible light. These demonstrated that B doping drove the response to the visible light, agreeing well with the results from XRD, XPS, and DRS, which B doping modified the electronic structure around the conduction band edge of TiO_2, led to the band gap narrow, and consequently caused the as-prepared boron/ferrum/cerium/titania photocatalyst response to visible light. The results revealed that impurities Fe and Ce, which ferrum and cerium atoms existed in the forms FeO/Fe_2O_3 and Ce_2O_3/CeO_2, dispersed on the surface of TiO_2, increased efficiently the photoatalytic activity.

According to the reports [12,19], the possible mechanism that Fe and Ce impurities improve the photocatalytic performance is as follows: Fe^{3+} is very stable because of its half-filled electronic configuration. When degradation DCP, Fe^{3+} ion trapped an electron to change into Fe^{2+}, thus demolishing the electronic configuration. For the purpose of maintaining steady structure, the trapped electron could rapidly be transferred from Fe^{2+} to the oxygen molecules adsorbed on the surface of the photocatalyst and Fe^{2+} recurred to the original half-filled state (Fe^{3+}), thus accelerating charge transfer, promoting effectively the separation of the electrons and holes and prohibiting their recombination. Additionally, because the ionic radius of Ti^{4+} is much than that of Ce^{3+} or Ce^{4+}, titanium atoms could enter into the lattice and replaced Ce^{3+} or Ce^{4+}. As a result

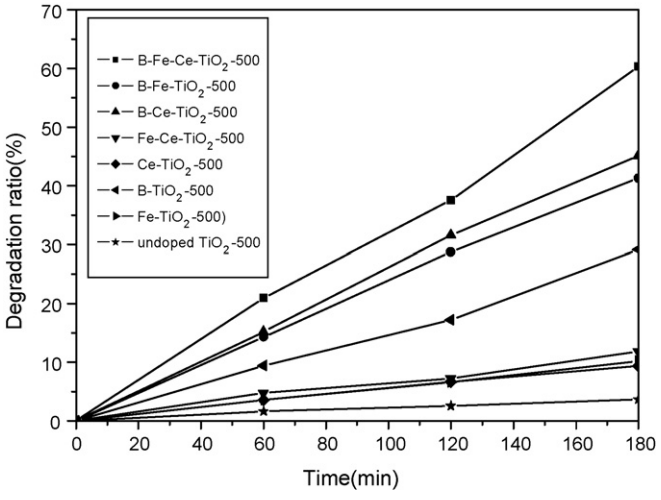

Fig. 11. Temporal course of visible-light-driven photocatalytic degradation of DCP.

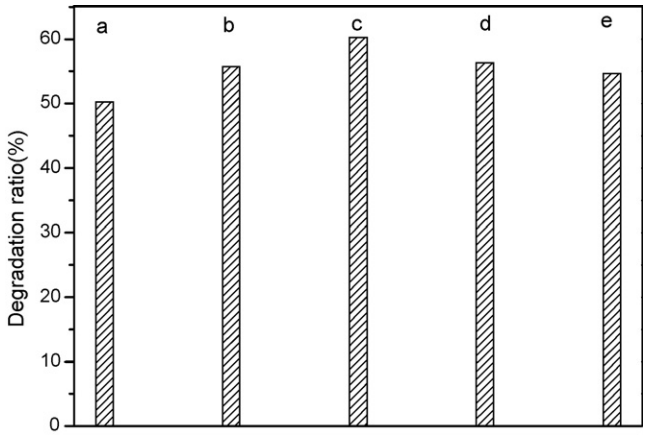

Fig. 12. Under visible illumination after reaction for 3 h the degradation DCP ratios: (a) B–Fe–Ce–TiO_2-400, (b) B–Fe–Ce–TiO_2-450, (c) B–Fe–Ce–TiO_2-500, (d) B–Fe–Ce–TiO_2-550, and (e) B–Fe–Ce-TiO_2-600.

of substitution, a charge balance was destroyed. In order to keep the equilibrium, more hydroxide ions would be adsorbed onto the surface, thus benefiting the photo-generated electron–hole pairs separation, preventing effectively their recombination, and bring about eventually the increase of the photoactivity. Therefore, Fe and Ce could increase the photocatalytic performance. The results of comparative tests for degradation of DCP suggested that the cooperative actions of boron, ferrum and cerium resulted in the increase of the photoactivity.

Fig. 12 shows the degradation ratios of DCP after reaction for 3 h over boron/ferrum/cerium/titania photocatalyst annealed at different temperature under visible illumination. It could be seen that the calcination temperature had an effect on the photocatalytic activity of the as-prepared samples and B–Fe–Ce–TiO_2-500 represented the best photoactivity among these samples. Generally, many factors, e.g., surface area, crystallinity, and surface hydroxyl densities influence the activity of a photocatalyst [32–35]. However, because these factors are closely related to each other, the photocatalytic activity is a combined effect of many factors. Therefore, it is not surprising that the highest photocatalytic performance was achieved at a particular calcination temperature.

For the purpose of testing the stability of the sample B–Fe–Ce–TiO_2-500, four cycles of photocatalytic experiments under visible irradiation were carried out and it was found that the photocatalytic performance did not decrease. In addition, the sample B–Fe–Ce–TiO_2-500 after the photocatalytic reaction was used to determine XPS and it was found that there was no difference between the peaks of the sample before and after the catalytic reaction, indicating that boron/ferrum/cerium/titania photocatalyst did not suffer the instability.

4. Conclusions

The boron/ferrum/cerium/titania photocatalyst having narrow band gap, showing strong photoabsorption and exhibiting high activity in the visible region was prepared. Its microcrystal only contained anatase phase and presented approximately spherical shape. It was testified that boron was weaved into the crystal structure of TiO_2 and the crystal lattice locally was distorted by incorporating boron, which could narrow the band gap of TiO_2. The ferrum and cerium presented in the forms of FeO/Fe_2O_3 and Ce_2O_3/CeO_2, and dispersed on the face of TiO_2, which could prohibit the electrons and holes recombination and increased photo-quantum efficiency. It was also verified that the impurities could retard phase transformation of TiO_2, prohibit growth

of microcrystalline, and facilitated forming the photocatalyst with large BET surface area. The synergistic effects of boron, ferrum and cerium were responsible for the visible light response and high photoactivity.

References

[1] R.I. Bickley, F.S. Stone, J. Catal. 31 (1973) 389–397.
[2] E. Borgarello, J. Kiwi, M. Gratzel, E. Pelizzetti, M. Visca, J. Am. Chem. Soc. 104 (1982) 2996–3002.
[3] M.D. Ward, A.J. Bard, J. Phys. Chem. 86 (1982) 3599–3605.
[4] M. Huang, E. Tso, A. Datye, Environ. Sci. Technol. 30 (1996) 3084–3088.
[5] J. Matos, J. Laine, J.M. Herrmann, Appl. Catal. B: Environ. 18 (1998) 281–291.
[6] R. Asahi, T. Morikawa, T. Ohwaki, K. Aoki, Y. Taga, Science 293 (2001) 269–271.
[7] S.U.M. Khan, M. Al-Shahry, W.B. Ingler Jr., Science 297 (2002) 2243–2245.
[8] S. Sakthivel, H. Kisch, Angew. Chem. Int. Ed. 42 (2003) 4908–4911.
[9] T. Ohno, M. Akiyoshi, T. Umebayashi, K. Asai, T. Mitsui, M. Matsumura, Appl. Catal. A: Gen. 265 (2004) 115–121.
[10] W. Ho, J.C. Yu, S. Lee, Chem. Commun. (2006) 1115–1117.
[11] H. Choi, A.C. Sofranko, D.D. Dionysiou, Adv. Funct. Mater. 16 (2006) 1067–1074.
[12] A.W. Xu, Y. Gao, H.Q. Liu, J. Catal. 207 (2002) 151–157.
[13] U. Siemon, D. Bahnemanna, J.J. Testa, D. Rodrıguez, M.I. Litter, N. Bruno, J. Photochem. Photobiol. A: Chem. 148 (2002) 247–255.
[14] K. Wilke, H.D. Breuer, J. Photochem. Photobiol. A: Chem. 121 (1999) 49–53.
[15] D. Robert, Catal. Today 122 (2007) 20–26.
[16] S. Liu, J.H. Yang, J.H. Choy, J. Photochem. Photobiol. A: Chem. 179 (2006) 75–80.
[17] W. Zhao, W.H. Ma, C.C. Chen, J.C. Zhao, Z.G. Shuai, J. Am. Chem. Soc. 126 (2004) 4782–4783.
[18] Y. Sakatani, J. Nunoshige, H. Ando, K. Okusako, H. Koike, T. Takata, J.N. Kondo, M. Hara, K. Domen, Chem. Lett. 32 (2003) 1156–1157.
[19] Z.H. Yuan, J.H. Jia, L.D. Zhang, Mater. Chem. Phys. 73 (2002) 323–326.
[20] D. Li, H. Haneda, S. Hishita, N. Ohashi, Chem. Mater. 17 (2005) 2596–2602.
[21] X.W. Zhang, M.H. Zhou, L.C. Lei, Catal. Commun. 7 (2006) 427–431.
[22] D.J. Joyner, D.M. Hercules, J. Chem. Phys. 72 (1980) 1095–1108.
[23] J.A. Schreifels, P.C. Maybury, W.E. Swartz, J. Catal. 65 (1980) 195–206.
[24] G. Mavel, J. Escard, P. Costa, J. Castaing, Surf. Sci. 35 (1973) 109–116.
[25] D.J. Joyner, O. Johnson, D.M. Hercules, J. Am. Chem. Soc. 102 (1980) 1910–1917.
[26] P. Mills, J.L. Sullivan, J. Phys. D: Appl. Phys. 16 (1983) 723–732.
[27] N.S. McIntyre, D.G. Zetaruk, Anal. Chem. 49 (1977) 1521–1529.
[28] G. Praline, B.E. Koel, R.L. Hance, H.I. Lee, J.M. White, J. Electron Spectrosc. Relat. Phenom. 21 (1980) 17–30.
[29] F.B. Li, X.Z. Li, M.F. Hou, K.W. Cheah, W.C.H. Choy, Appl. Catal. A: Gen. 285 (2005) 181–189.
[30] T. Umebayashi, T. Yamaki, H. Itoh, K. Asai, Appl. Phys. Lett. 81 (2002) 454–456.
[31] K.S. Yang, Y. Dai, B.B. Huang, Phys. Rev. B 76 (2007) 195201.
[32] T.H. Tran, A.Y. Nosaka, Y. Nosaka, J. Photochem. Photobiol. A: Chem. 192 (2007) 105–113.
[33] Y. Ohko, K. Hashimoto, A. Fujishima, J. Phys. Chem. A 101 (1997) 8057–8062.
[34] J. Lukáč, M. Klementová, P. Bezdička, S. Bakardjieva, J. Šubrt, L. Szatmáry, Z. Bastl, J. Jirkovský, Appl. Catal. B-Environ. 74 (2007) 83–91.
[35] C. Xie, Q. Yang, Z. Xu, X. Liu, Y. Du, J. Phys. Chem. B 110 (2006) 8587–8592.